

Time Variability of the Neutral Iron Lines from the Sgr B2 Region and its Implication of a Past Outburst of Sgr A*

Tatsuya INUI, Katsuji KOYAMA, Hironori MATSUMOTO and Takeshi Go TSURU
Department of Physics, Graduate School of Science, Kyoto University, Sakyo-ku, Kyoto 606-8502
inuit@cr.scphys.kyoto-u.ac.jp

(Received 2008 January 15; accepted 2008 February 29)

Abstract

We investigate long-term X-ray behaviors from the Sgr B2 complex using archival data of the X-ray satellites Suzaku, XMM-Newton, Chandra and ASCA. The observed region of the Sgr B2 complex includes two prominent spots in the Fe I K- α line at 6.40 keV, a giant molecular cloud M 0.66–0.02 known as the “Sgr B2 cloud” and an unusual X-ray source G 0.570–0.018. Although these 6.40 keV spots have spatial extensions of a few pc scale, the morphology and flux of the 6.40 keV line has been time variable for 10 years, in contrast to the constant flux of the Fe XXV-K α line at 6.67 keV in the Galactic diffuse X-ray emission. This time variation is mostly due to M 0.66–0.02; the 6.40 keV line flux declined in 2001 and decreased to 60% in the time span 1994–2005. The other spot G 0.570–0.018 is found to be conspicuous only in the Chandra observation in 2000. From the long-term time variability (~ 10 years) of the Sgr B2 complex, we infer that the Galactic Center black hole Sgr A* was X-ray bright in the past 300 year and exhibited a time variability with a period of a few years.

Key words: Galaxy:center — ISM:clouds — ISM:individual (Sagittarius B) — X-rays:individual (Sagittarius B) — X-rays:ISM

1. Introduction

Our Galactic Center (GC) black hole, Sgr A*, has a mass of $4 \times 10^6 M_\odot$ (Eisenhauer et al. 2005; Ghez et al. 2005), but is quiescent with an X-ray luminosity of only 10^{33-34} ergs s $^{-1}$ (Baganoff et al. 2001), which is many orders of magnitude smaller than that of canonical AGNs. Sgr A* has been also found to exhibit frequent X-ray flares (e.g., Baganoff et al. 2001). This X-ray flare activity is not huge, however, with a typical duration of 10 ks and an amplitude that is only a factor of ten above the non-flare phase. Therefore, even at the flare peak, the X-ray luminosity is $\sim 10^6$ times lower than the Eddington luminosity of this supermassive black hole.

The 6.40 keV line features in molecular clouds suggest an active phase in the past. The Sgr B complex of giant molecular clouds emit peculiar X-rays with a strong K-shell transition line at 6.40 keV from neutral iron (equivalent width of 1–2 keV) and a deep absorption edge at 7.1 keV (equivalent N_H of 10^{23-24}) (Koyama et al. 1996). The 6.40 keV line flux and the spectrum necessitate the existence of strong X-ray sources irradiating the clouds. The detailed X-ray morphology of the neutral iron line in the Sgr B2 cloud has been investigated by Chandra and it was found that the external source is likely to be located in the GC direction (Murakami et al. 2001b). However, no such source has been found, neither toward the GC, nor in regions near the GC. Based on these results, Koyama et al. (1996), Murakami et al. (2001b) and Koyama et al. (2007b) proposed that the Sgr B2 complex contains X-ray reflection nebulae (XRNe) irradiated by Sgr A*, which must have been six orders of magnitude X-ray brighter

about 300 years ago, which is the light travel time between Sgr B2 and Sgr A*. Other molecular clouds such as M 0.74–0.09, Sgr B1, Sgr C and M 0.11–0.08 also have intense 6.40 keV lines (Koyama et al. 2007b, Nobukawa et al. 2008, Murakami et al. 2001a, Yusef-Zadeh et al. 2007). Some, if not all, of them, are also likely to be XRNe (Koyama et al. 2007b, Nobukawa et al. 2008, Murakami et al. 2001a).

Since the 6.40 keV line can be also produced by high-energy electrons bombarding the cloud (Tatischeff 2003), Predehl et al. (2003) and Yusef-Zadeh et al. (2007) argued against the XRNe scenario and proposed electron bremsstrahlung instead. One way to distinguish between these two possible scenarios (i.e., irradiation by X-rays or electrons (charged-particles)) would be to detect the time variability of the 6.40 keV line.

Muno et al. (2007) discovered the time variability of the 6.40 keV line clumps in the molecular cloud M 0.11–0.11. Koyama et al. (2008a) also found changes in the flux and morphology of the 6.40 keV line of the Sgr B2 complex between the Chandra and Suzaku observations in 2000 and 2005, respectively.

Since variability over a few years from a pc-scale object requires light-speed communication, charged particles are unlikely to be the origin of the 6.40 keV line. This time variability, on the other hand, supports the XRNe scenario; X-rays from external sources irradiate molecular clouds and produce the fluorescence iron line at 6.40 keV and Thompson scattering continuum emission in the same manner as an X-ray echo. Using the time variable X-ray echo, we can infer the light curve of Sgr A* in the past.

This paper reports a comprehensive X-ray study based

on all the available archival data of the Sgr B2 complex (i.e., the ASCA, Chandra, XMM-Newton and Suzaku data). We derived a 10-year-scale light curve for the 6.40 keV line. We found the time variability of the 6.40 keV line from the Sgr B2 complex by using the time-constant 6.67 keV line from the GC diffuse X-rays (GCDX) as a reference. In this paper, the distance to the Sgr B2 complex is assumed to be 8.5 kpc (Reid et al. 1988).

2. Observations and Data Reduction

We used four deep exposure and two short survey observations as listed in table 1. However, for imaging analysis we used only the deep exposure observations.

2.1. *Suzaku*

The Sgr B2 complex was observed with the XIS on 10–12 October 2005. The XIS consists of four sets of X-ray CCD camera systems (XIS0, 1, 2, and 3) placed on the focal planes of four X-ray telescopes (XRTs) on board the Suzaku satellite. XIS0, 2 and 3 have front-illuminated (FI) CCDs, whereas XIS1 has a back-illuminated (BI) CCD. Detailed descriptions of the Suzaku satellite, XRT and XIS are found in Mitsuda et al. (2007), Serlemittos et al. (2007) and Koyama et al. (2007a). The XIS observation was made in the normal mode. The effective exposure time after removing the epoch of the low earth elevation angle ($ELV \leq 5^\circ$) and the South Atlantic Anomaly was about 89 ks. We analyzed the data using the software package HEASoft 6.2. The XIS gain was fine-tuned using the same procedures described in Koyama et al. (2007b). Using point sources in the field, we re-registered the absolute astrometry by shifting ($-0^\circ0001$, $-0^\circ0062$) in the (l , b) coordinate, referring the Chandra point-source positions (Koyama et al. 2007b).

2.2. *XMM-Newton*

The X-ray data were obtained using the European Photon Imaging Camera (EPIC) (Strüder et al. 2001; Turner et al. 2001) onboard the XMM-Newton on 1 April 2001 and 4 September 2004. The observations were performed in extended full-frame mode. The data were analyzed using Science Analysis Software (SAS 7.1.0). Event files for both the PN and the Metal Oxide Semiconductor (MOS) detectors were produced using the epproc and emproc tasks of SAS, respectively. The event files were screened for high particle-background periods. In our analysis, we dealt only with events corresponding to patterns 0–4 for the PN and 0–12 for the MOS instruments. For the observation in 2004, we made the total band images (0.3–10 keV) for each detector and detected point sources (93 point sources from MOS1, 97 from MOS2, and 111 from PN). 27 sources were detected with all three detectors within positional uncertainties of 10 arcsec, the sizes of PSF of EPIC at 6 keV, and 19 sources have possible counterparts with catalogued point sources of Chandra (Muno et al. 2003). The mean position difference of these point sources relative to the

Chandra positions is ($-0^\circ0006$, $0^\circ0003$) in celestial coordinates. We fine-tuned the XMM-Newton frame by shifting $(\Delta\alpha, \Delta\delta) = (0^\circ0006, -0^\circ0003)$.

2.3. *Chandra*

Sgr B2 was observed using the Advanced CCD Imaging Spectrometer (ACIS-I) onboard the Chandra observatory (Weisskopf et al. 2002) on 29 March 2000 and 16 July 2001. We used the event files provided by standard pipeline processing. Only the grade 0, 2, 3, 4, and 6 events were used in the analysis. Each CCD chip subtends an 8.3-arcmin square in the sky, while the pixel size is 0.5 arcsec. The on-axis spatial resolution is 0.5-arcsec (full width at half-maximum (FWHM)). Images, spectra, ancillary files and response matrices were created using the software CIAO v3.4. The absolute positional accuracy is 0.6 arcsec (Weisskopf et al. 2003).

2.4. *ASCA*

The ASCA observations of Sgr B2 were performed on 22 and 24 September 1994 for ~ 80 ks in total. We used the event files provided by standard pipeline processing. We merged the two observation data since the observation dates and aim points are almost the same. Since the GIS data did not have sufficient energy resolution (~ 470 eV at 5.9 keV) to separate the iron lines, we used only SIS data for the analysis. Unlike Suzaku and XMM-Newton, no available point sources to use as a reference for Chandra for the absolute astrometry correction were found. Therefore, the astrometric uncertainty of SIS image remains about 40 arcsec¹. We used the software package HEASoft 6.2 in the analysis.

3. Analysis

3.1. *Spectra of the Sgr B2 region*

Figure 1 shows relevant diffuse sources in the Sgr B2 complex overlaid on the XMM-Newton 6–7 keV image. Since the FOVs and pointing positions of the Suzaku, Chandra, XMM-Newton and ASCA observations are slightly different from each other, we selected a region in which all the observed areas overlapped (referred to hereafter as the Sgr B2 region). The Sgr B2 region (the overlapping region) is indicated by the solid squares in figure 1. The subsequent data analysis and discussion are based on the sources in the Sgr B2 region. Hereafter, we refer to the Sgr B2 cloud as M 0.66–0.02. G 0.61+0.01 is a new source with a strong 6.67 keV line, hence possibly a new young SNR (Koyama et al. 2007b). G 0.570–0.0018 is an unusual diffuse source discovered by Senda et al. 2002. M 0.74–0.09 is also a new 6.40 keV source, but it is not discussed in this paper, because it is outside of the Sgr B2 region.

We extracted X-ray spectra from the Sgr B2 region and subtracted the off-plane blank-sky regions. Thus, the cosmic X-ray background (CXB) and non-X-ray background (NXB) were subtracted but the GCDX were not sub-

¹ See http://heasarc.gsfc.nasa.gov/docs/asca/cal_probs.html

Table 1. Observation Log

| Observatory | Obs. ID | Date (yyyy/mm/dd) | Exposure Time (sec) |
|-------------|------------|----------------------|------------------------|
| ASCA | 52006000 | 1994/09/22 | 58,395 |
| ASCA | 52006001 | 1994/09/24 | 21,500 |
| Chandra | 944 | 2000/03/29 | 98,629 |
| XMM-Newton | 0112971501 | 2001/04/01 | 12,649 |
| Chandra | 2280 | 2001/07/16 | 10,423 |
| XMM-Newton | 0203930101 | 2004/09/04 | 42,282 |
| Suzaku | 100037060 | 2005/10/10 | 89,072 |

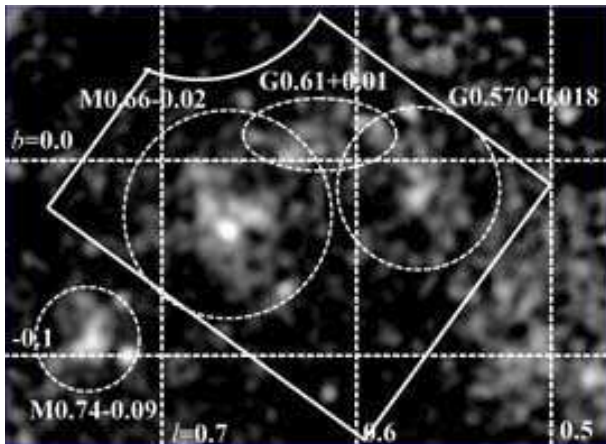


Fig. 1. XMM-Newton image in the 6–7 keV band. The solid line indicates the selected area of the Sgr B2 complex (see text). The dashed circles are the individual diffuse sources discussed in this paper. M0.66–0.02 is the Sgr B2 cloud. G0.61+0.01 is a new source with a strong 6.67 keV line, possibly a new young SNR. G0.570–0.0018 is an unusual diffuse source.

tracted. As the off-plane blank-sky, we selected the north ecliptic pole data for XIS, distributed blank-sky databases for MOS and ACIS, and Lockman hole data for PN and SIS.

The blank-sky-subtracted spectra are shown in figure 2. These spectra exhibit continuum emissions and pronounced peaks due to Fe I $K\alpha$ (6.40 keV), Fe XXV $K\alpha$ (6.67 keV), and the composite of Fe XXVI $K\alpha$ (6.96 keV) and Fe I $K\beta$ (7.06 keV). The continuum emission is composed of: 1) the continuum of the GCDX (Koyama et al. 2007c), 2) the continuum (thermal bremsstrahlung) from G0.61+0.01, a new SNR in this region (Koyama et al. 2007b), and 3) a non-thermal power-law continuum with a deep iron K-edge related to the 6.40 keV line (Koyama et al. 1996).

It is practically impossible to resolve these three continuums; we therefore represented these three continuum by a single power-law continuum with absorption (the `wabs*power-law` model in the `xspec` code). We then added four K-shell lines by Gaussian functions. These are the Fe XXV $K\alpha$ (\sim 6.67 keV) and Fe XXVI $K\alpha$ (\sim 6.96 keV) lines due to the GCDX, and Fe I $K\alpha$ (6.40 keV) and Fe I $K\beta$ (7.06 keV) lines due mainly to the Sgr B2 region. Thus,

the model spectrum in the `xspec` code is given as;

$$\text{wabs*power-law} + 4 \text{ Gaussians} \quad (1)$$

3.1.1. Suzaku

The spectra of the Sgr B2 region and background subtractions of the blank sky for XIS 0,1,2 and 3 were performed separately, however all the FI-CCD spectra (XIS0, 1 and 3) were combined, because their response functions are almost identical with each other. We fitted the FI-CCD and BI-CCD spectra simultaneously in the energy band of 5–8 keV with the model given by equation (1). All the parameters were free under the following constraints: the line widths were fixed to be 0 eV except that of the Fe XXV $K\alpha$ line (Koyama et al. 2007c), and the energy interval between Fe I $K\alpha$ (6400 eV) and $K\beta$ (7058 eV) was fixed at the theoretical value of 658 eV (Kaastra & Mewe 1993). The best-fit spectra for the FI and BI are shown in figures 2(a) and 2(b) respectively, while the best-fit parameters are listed in table 2.

Although the K-shell lines from highly ionized iron, the Fe XXVI $K\alpha$ and Fe XXV $K\alpha$ lines are due to the largely extended GCDX, the best-fit center energy of the Fe XXVI $K\alpha$ line (6665 eV) and the flux ratio of Fe XXVI $K\alpha$ to Fe XXV $K\alpha$ (0.30) are slightly smaller than those (6680 eV and 0.34, respectively) found in the GC region (Koyama et al. 2007c). This may be due to the contamination of a strong Fe XXV $K\alpha$ line of a new SNR G0.61+0.01 (Koyama et al. 2007b).

When fitting the XMM-Newton, Chandra and ASCA spectra, we fixed the line centroids and the $K\alpha$ flux ratio of Fe XXVI and Fe XXV to the best-fit Suzaku values given in table 2, because the statistics and energy response of these satellites were limited compared to Suzaku.

3.1.2. XMM-Newton

We fitted the MOS and PN spectra separately, where the line center energies and the $K\alpha$ line flux ratio of Fe XXVI and Fe XXV were fixed to those of the Suzaku best-fit values (see Section 3.1.1). This fit failed in reproducing the line and edge structures in the PN spectra, indicating a systematic gain shift; we thus added a gain offset as a free parameter. The fit was then acceptable as Table 3 shows. The best-fit spectra are given in figures 2(c)–(f).

3.1.3. Chandra

We fitted the Chandra spectra using the same method as the XMM-Newton case. The spectrum in 2000 was well

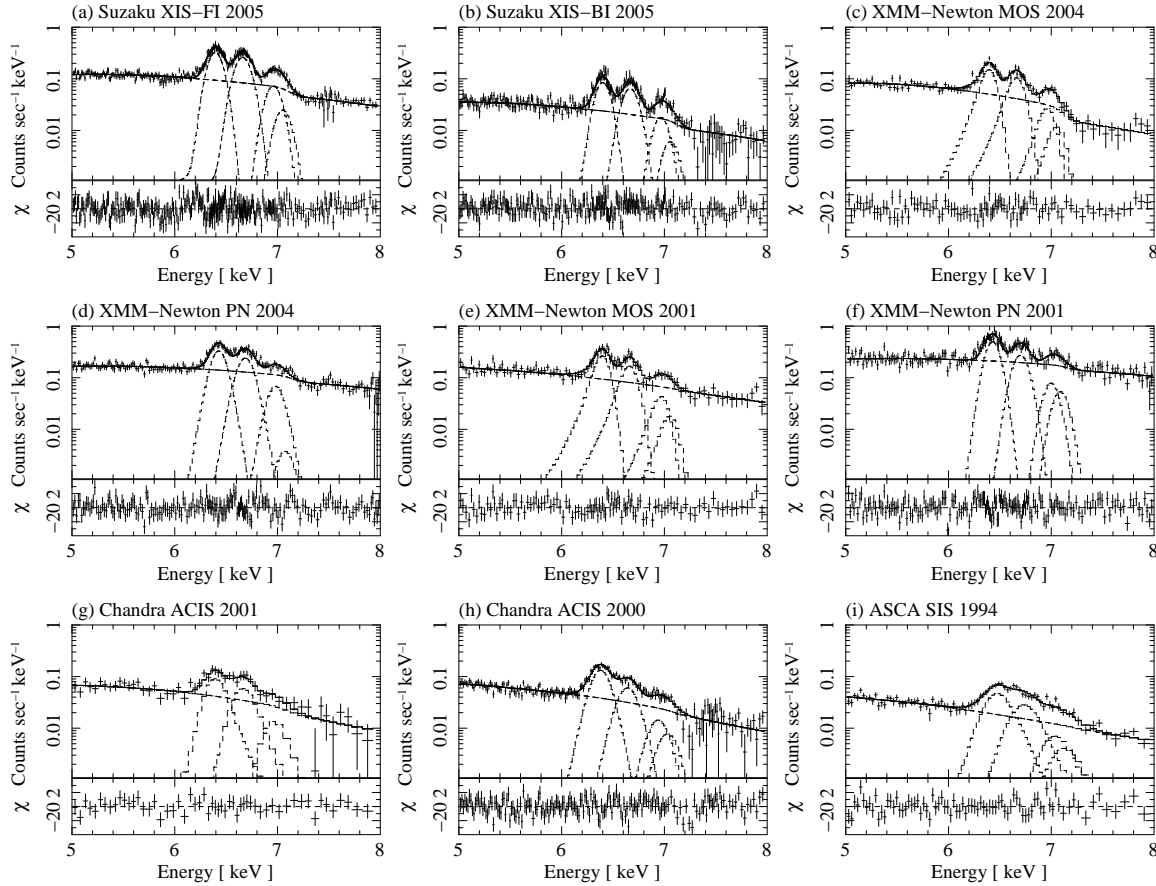


Fig. 2. The blank-sky-subtracted spectra of the Sgr B2 region, with the Suzaku XIS FI sensors (a) and BI sensor (b) in 2005, XMM-Newton MOS (c) and PN (d) in 2004, (e) and (f) in 2001, Chandra ACIS-I (g) in 2001 and (h) in 2000, and ASCA SIS (i) in 1994. The solid lines indicate the best-fit models (see text).

fitted by adding a gain offset of ~ -20 eV. The best-fit spectra and parameters are given in figure 2(g) and table 3. In the 2001 spectra, however, the best-fit photon index was unrealistic with $\Gamma \sim -2.2$. If we fixed $\Gamma = 2.6$, the best-fit Suzaku value, then there were large residuals above the 7 keV band. We compared the count rates in the 10.0–12.5 keV band between the source and blank-sky spectra, and found that the high-energy band count-rate of the blank-sky was 2.4 times smaller than that of the source spectra. Thus, the strange behaviors are likely due to unstable NXB. We therefore subtracted the blank-sky spectra by first multiplying them by a factor of 2.4. We then obtained a good fit with reasonable parameters. The best-fit spectra and parameters are shown in figure 2(h) and table 3, respectively. It could be argued that the background subtraction described above is artificial, and hence may cause large systematic errors in the line flux. However, the line flux errors for the different background subtractions are within 10%. More details concerning the line flux dependence on the continuum shape and/or background subtractions are given in Section 3.2.2, for the case of the XMM-Newton (table 5).

3.1.4. ASCA

The fitting procedures for the ASCA spectra were the same as those for XMM-Newton and Chandra spectra.

The ASCA spectra require a large systematic gain offset about 80 eV to adjust the iron line centroids. This large offset is caused by chip-to-chip variation of the gain². The best-fit spectra and parameters are shown in figure 2(i) and in table 3.

3.2. Systematic Errors of the Line Flux

The estimation of the line flux depends on the underlying continuum shape and the background subtraction. We thus examined the possible systematic error cause by the assumed continuum and background subtraction.

3.2.1. Dependence of the Line Flux on the Continuum Shape

We fixed either Γ (Case 2) or N_{H} (Case 3) or both (Case 4) to those of the best-fit Suzaku results and fitted the XMM-Newton, Chandra and ASCA spectra. For comparison, we call fitting with free Γ and N_{H} as Case 1. The best-fit parameters of these fittings (Cases 2, 3, and 4) are shown in table 4.

From table 4, we find that the best-fit fluxes of the 6.40 keV and 6.67 keV lines for the four fitting cases are consistent within $\pm 5\%$ with each other, which is smaller than the statistical errors. We therefore ignore these sys-

² See <http://heasarc.gsfc.nasa.gov/docs/asca/4ccd.html>

Table 3. The XMM-Newton, Chandra and ASCA fitting results for the Sgr B2 region

| Observatory Detector | XMM-Newton | | XMM-Newton | | Chandra | | ASCA |
|-----------------------------|------------------------|------------------------|------------------------|------------------------|------------------------|------------------------|------------------------|
| | MOS(2004) | PN(2004) | MOS(2001) | PN(2001) | ACIS(2001) | ACIS(2000) | SIS(1994) |
| —Continuum— | | | | | | | |
| N_H | $5.3^{+1.4}_{-1.3}$ | $2.1^{+0.4}_{-0.4}$ | $0.5^{+1.3}_{-0.5}$ | $1.5^{+1.0}_{-0.9}$ | $2.4^{+3.4}_{-2.4}$ | $1.0^{+0.5}_{-0.4}$ | $0.7^{+1.0}_{-0.7}$ |
| Γ | $3.6^{+0.7}_{-0.7}$ | $1.6^{+0.2}_{-0.1}$ | $0.4^{+0.6}_{-0.5}$ | $0.9^{+0.4}_{-0.4}$ | $1.0^{+1.7}_{-1.5}$ | $0.7^{+0.4}_{-0.5}$ | $1.1^{+0.7}_{-0.5}$ |
| F_{pow} | $4.8^{+0.2}_{-0.2}$ | $7.0^{+0.2}_{-0.2}$ | $8.8^{+0.4}_{-0.4}$ | $9.4^{+0.3}_{-0.3}$ | $7.2^{+0.5}_{-0.5}$ | $6.7^{+0.2}_{-0.2}$ | $5.8^{+0.2}_{-0.2}$ |
| —Neutral iron lines— | | | | | | | |
| F_{640} | $1.03^{+0.08}_{-0.08}$ | $1.06^{+0.05}_{-0.07}$ | $1.52^{+0.15}_{-0.16}$ | $1.27^{+0.11}_{-0.12}$ | $1.37^{+0.26}_{-0.26}$ | $1.71^{+0.08}_{-0.08}$ | $1.63^{+0.18}_{-0.17}$ |
| F_{706} | $0.13^{+0.07}_{-0.07}$ | $0.15^{+0.05}_{-0.15}$ | $0.16^{+0.16}_{-0.14}$ | $0.17^{+0.09}_{-0.09}$ | $0.10^{+0.32}_{-0.10}$ | $0.17^{+0.09}_{-0.04}$ | $0.22^{+0.15}_{-0.13}$ |
| —Highly ionized iron lines— | | | | | | | |
| F_{667} | $0.91^{+0.04}_{-0.08}$ | $0.89^{+0.06}_{-0.06}$ | $1.22^{+0.15}_{-0.16}$ | $0.81^{+0.11}_{-0.11}$ | $1.14^{+0.27}_{-0.27}$ | $1.00^{+0.08}_{-0.07}$ | $1.20^{+0.18}_{-0.18}$ |
| δ_{Gain}^a | 0(fix) | 21^{+3}_{-3} | 0(fix) | 35^{+4}_{-11} | 0(fix) | -20^{+4}_{-3} | 71^{+21}_{-13} |
| χ^2/dof | 88.9/93 | 185.6/169 | 84.2/101 | 260.4/164 | 37.5/50 | 196.0/169 | 81.8/76 |

Note—Terminologies and units are same as table 2.

The intensity of Fe XXVI $K\alpha$ is fixed at 30% of that of Fe XXV $K\alpha$ determined by the Suzaku fit.

The other parameters are fixed to the best-fit Suzaku values.

^a Fine-tuning offset energy in units of eV.

Table 2. The best-fit Suzaku (XIS) results of the Sgr B2 region

| Parameter | Terminology | Value |
|--|---------------------|------------------------|
| —Continuum— | | |
| Absorption ^a | N_H | $3.0^{+0.3}_{-0.5}$ |
| Photon index | Γ | $2.6^{+0.2}_{-0.2}$ |
| Power-law flux ^b | F_{pow} | $5.2^{+0.4}_{-0.4}$ |
| —Neutral iron lines— | | |
| Center energy of Fe I- $K\alpha$ ^c | E_{640} | 6400^{+4}_{-1} |
| Flux of Fe I- $K\alpha$ ^d | F_{640} | $1.14^{+0.04}_{-0.03}$ |
| Center energy of Fe I- $K\beta$ ^c | E_{706} | 7058^f |
| Flux of Fe I- $K\beta$ ^d | F_{706} | $0.11^{+0.05}_{-0.07}$ |
| —Highly ionized iron lines— | | |
| Center energy of Fe XXV- $K\alpha$ ^c | E_{667} | 6665^{+4}_{-3} |
| Width of Fe XXV- $K\alpha$ ^e | σ_{667} | 27^{+7}_{-9} |
| Flux of Fe XXV- $K\alpha$ ^d | F_{667} | $1.07^{+0.04}_{-0.05}$ |
| Center energy of Fe XXVI- $K\alpha$ ^c | E_{697} | 6966^{+14}_{-13} |
| Flux of Fe XXVI- $K\alpha$ ^d | F_{697} | $0.32^{+0.05}_{-0.04}$ |
| | χ^2/dof | 574.4/514 |

Note—Parentheses indicate the 90% confidence limit.

^a In unit of 10^{23} H cm⁻².

^b Observed flux of a power-law continuum in the 5–8 keV band in unit of 10^{-4} photons cm⁻² s⁻¹.

^c Line center energy in unit of eV.

^d Observed line flux in unit of 10^{-4} photons cm⁻² s⁻¹.

^e Line width in the Gaussian sigma in unit of eV.

^f The energy gap between $K\alpha$ (6400 eV) and $K\beta$ (7058 eV) is fixed at the theoretical value (+658 eV) (Kaastra & Mewe 1993).

tematic errors, and refer to the Case 1 parameters in the subsequent discussion.

3.2.2. Dependence of the Line Flux on the Background Subtraction

As we have already noted, the NXB of Chandra in the 2001 observation was unusually high. This unstable (time-dependent) NXB is also often the problem in XMM-Newton analysis (Carter & Read 2007). The unstable NXB and associated lines may affect the estimated line fluxes in the source spectra. To check these systematic errors, we derived the count rates of MOS and PN for the source and background above the 10 keV band, where NXB is dominant. The count-rate ratios between the source and background were used as correction factors α for the background. The factors α for the XMM-Newton data in 2004 are relatively small, 1.0 and 1.4 for MOS and PN, respectively, while those for the data in 2001 are 2.1 and 2.6 for MOS and PN, respectively.

We multiplied the background spectra by the factors α , subtracted them from the source spectra, and then fitted them with the model expressed by equation (1) for the four cases (Case 1 to 4). The results are shown in table 5. In this process, the CXB was also multiplied by the factor α . Therefore, we over(under)-subtracted the CXB by the factor α . The surface brightness of the CXB with a typical Galactic absorption of 6×10^{22} cm⁻² is $\sim 10^{-15}$ ergs cm⁻² s⁻¹ arcmin⁻² in the Sgr B2 region, which is only a few percent of the continuum flux in the region. Thus, possible over(under)-subtraction of the CXB can be neglected in the following discussion.

From tables 4 and 5, we find that the fluxes of the 6.40 keV and 6.67 keV lines with corrected background subtraction (table 5) are almost the same as those with normal background subtraction (table 4) within the statistical errors, although the continuum flux is substantially different. Thus, in the following discussion based on the fluxes of the 6.40 keV and 6.67 keV lines, we can ignore possible uncertainty in the time-dependent back-

Table 4. Dependence of the best-fit flux on the continuum parameters for the Sgr B2 region

| | Parameter | Case1 | Case2 | Case3 | Case4 |
|--------------|------------------|------------------------|------------------------|------------------------|------------------------|
| —XMM-Newton— | | | | | |
| MOS(2004) | F_{pow} | $4.8^{+0.2}_{-0.2}$ | $4.9^{+0.2}_{-0.2}$ | $4.8^{+0.2}_{-0.2}$ | $4.8^{+0.2}_{-0.2}$ |
| | F_{640} | $1.03^{+0.08}_{-0.08}$ | $1.04^{+0.08}_{-0.08}$ | $1.07^{+0.07}_{-0.07}$ | $1.07^{+0.07}_{-0.07}$ |
| | F_{706} | $0.13^{+0.07}_{-0.07}$ | $0.10^{+0.07}_{-0.07}$ | $0.12^{+0.07}_{-0.07}$ | $0.12^{+0.07}_{-0.07}$ |
| | F_{667} | $0.91^{+0.04}_{-0.08}$ | $0.92^{+0.08}_{-0.04}$ | $0.95^{+0.07}_{-0.07}$ | $0.95^{+0.07}_{-0.07}$ |
| PN(2004) | F_{pow} | $7.0^{+0.2}_{-0.2}$ | $6.8^{+0.2}_{-0.2}$ | $7.1^{+0.2}_{-0.2}$ | $6.6^{+0.2}_{-0.2}$ |
| | F_{640} | $1.06^{+0.05}_{-0.07}$ | $1.02^{+0.08}_{-0.05}$ | $1.01^{+0.07}_{-0.05}$ | $1.07^{+0.06}_{-0.06}$ |
| | F_{706} | $0.15^{+0.05}_{-0.15}$ | $0.06^{+0.05}_{-0.06}$ | $0.10^{+0.05}_{-0.10}$ | $0.08^{+0.04}_{-0.05}$ |
| | F_{667} | $0.89^{+0.06}_{-0.06}$ | $0.88^{+0.05}_{-0.09}$ | $0.85^{+0.05}_{-0.06}$ | $0.92^{+0.05}_{-0.05}$ |
| MOS(2001) | F_{pow} | $8.8^{+0.4}_{-0.4}$ | $8.2^{+0.3}_{-0.3}$ | $8.9^{+0.4}_{-0.4}$ | $7.7^{+0.3}_{-0.3}$ |
| | F_{640} | $1.52^{+0.15}_{-0.16}$ | $1.53^{+0.12}_{-0.26}$ | $1.43^{+0.15}_{-0.16}$ | $1.55^{+0.14}_{-0.16}$ |
| | F_{706} | $0.16^{+0.16}_{-0.14}$ | $0.31^{+0.12}_{-0.22}$ | $0.16^{+0.14}_{-0.16}$ | $0.32^{+0.14}_{-0.14}$ |
| | F_{667} | $1.22^{+0.15}_{-0.16}$ | $1.16^{+0.17}_{-0.19}$ | $1.10^{+0.15}_{-0.15}$ | $1.28^{+0.14}_{-0.14}$ |
| PN(2001) | F_{pow} | $9.4^{+0.3}_{-0.3}$ | $9.2^{+0.3}_{-0.3}$ | $9.6^{+0.3}_{-0.3}$ | $8.6^{+0.3}_{-0.3}$ |
| | F_{640} | $1.27^{+0.11}_{-0.12}$ | $1.19^{+0.11}_{-0.11}$ | $1.21^{+0.11}_{-0.11}$ | $1.29^{+0.11}_{-0.10}$ |
| | F_{706} | $0.17^{+0.09}_{-0.09}$ | $0.19^{+0.09}_{-0.08}$ | $0.14^{+0.10}_{-0.08}$ | $0.28^{+0.09}_{-0.08}$ |
| | F_{667} | $0.81^{+0.11}_{-0.11}$ | $0.72^{+0.10}_{-0.10}$ | $0.73^{+0.10}_{-0.10}$ | $0.88^{+0.09}_{-0.10}$ |
| —Chandra— | | | | | |
| ACIS(2001) | F_{pow} | $7.2^{+0.5}_{-0.5}$ | $6.6^{+0.5}_{-0.5}$ | $7.1^{+0.5}_{-0.5}$ | $6.0^{+0.4}_{-0.4}$ |
| | F_{640} | $1.37^{+0.26}_{-0.26}$ | $1.36^{+0.27}_{-0.25}$ | $1.33^{+0.27}_{-0.24}$ | $1.48^{+0.24}_{-0.24}$ |
| | F_{706} | $0.10^{+0.32}_{-0.10}$ | $0.12^{+0.28}_{-0.12}$ | $0.12^{+0.32}_{-0.12}$ | $0.20^{+0.28}_{-0.20}$ |
| | F_{667} | $1.14^{+0.27}_{-0.27}$ | $1.16^{+0.27}_{-0.27}$ | $1.13^{+0.14}_{-0.41}$ | $1.30^{+0.24}_{-0.24}$ |
| ACIS(2000) | F_{pow} | $6.7^{+0.2}_{-0.2}$ | $6.0^{+0.2}_{-0.2}$ | $6.5^{+0.2}_{-0.2}$ | $5.7^{+0.2}_{-0.2}$ |
| | F_{640} | $1.71^{+0.08}_{-0.08}$ | $1.72^{+0.07}_{-0.10}$ | $1.67^{+0.08}_{-0.08}$ | $1.76^{+0.08}_{-0.08}$ |
| | F_{706} | $0.17^{+0.09}_{-0.04}$ | $0.26^{+0.12}_{-0.08}$ | $0.21^{+0.08}_{-0.09}$ | $0.31^{+0.09}_{-0.09}$ |
| | F_{667} | $1.00^{+0.08}_{-0.07}$ | $1.02^{+0.09}_{-0.08}$ | $0.97^{+0.08}_{-0.07}$ | $1.08^{+0.07}_{-0.08}$ |
| —ASCA— | | | | | |
| SIS(1994) | F_{pow} | $5.8^{+0.2}_{-0.2}$ | $5.5^{+0.2}_{-0.2}$ | $5.8^{+0.2}_{-0.2}$ | $5.4^{+0.2}_{-0.2}$ |
| | F_{640} | $1.63^{+0.18}_{-0.17}$ | $1.65^{+0.16}_{-0.18}$ | $1.62^{+0.14}_{-0.19}$ | $1.65^{+0.17}_{-0.10}$ |
| | F_{706} | $0.22^{+0.15}_{-0.13}$ | $0.30^{+0.17}_{-0.15}$ | $0.24^{+0.13}_{-0.15}$ | $0.30^{+0.17}_{-0.14}$ |
| | F_{667} | $1.20^{+0.18}_{-0.18}$ | $1.14^{+0.16}_{-0.18}$ | $1.07^{+0.18}_{-0.13}$ | $1.15^{+0.15}_{-0.16}$ |

Note—Same as table 3.

Case 1: N_{H} and Γ are free parameters (same as table 2 and 3)Case 2: N_{H} is a free parameter but Γ is fixed to the best-fit Suzaku value.Case 3: Γ is a free parameter but N_{H} is fixed to the best-fit Suzaku value.Case 4: N_{H} and Γ are fixed to the best-fit Suzaku value.

Table 5. Dependence of the XMM-Newton flux on the background-subtraction for the Sgr B2 region

| Parameter | Case1 | Case2 | Case3 | Case4 |
|---|------------------------|------------------------|------------------------|------------------------|
| XMM-Newton/PN(2004): Correction factor = 1.4 | | | | |
| F_{pow} | $5.5^{+0.2}_{-0.2}$ | $5.6^{+0.2}_{-0.2}$ | $5.5^{+0.2}_{-0.2}$ | $5.5^{+0.2}_{-0.2}$ |
| F_{640} | $1.05^{+0.06}_{-0.06}$ | $1.07^{+0.06}_{-0.06}$ | $1.08^{+0.06}_{-0.06}$ | $1.08^{+0.06}_{-0.06}$ |
| F_{706} | $0.06^{+0.05}_{-0.05}$ | $0.06^{+0.06}_{-0.05}$ | $0.07^{+0.05}_{-0.05}$ | $0.07^{+0.04}_{-0.06}$ |
| F_{667} | $0.90^{+0.05}_{-0.06}$ | $0.91^{+0.06}_{-0.06}$ | $0.92^{+0.06}_{-0.06}$ | $0.92^{+0.06}_{-0.06}$ |
| χ^2/dof | 238.4/169 | 240.9/170 | 240.7/170 | 241.1/171 |
| XMM-Newton/MOS(2001): Correction factor = 2.1 | | | | |
| F_{pow} | $3.9^{+0.3}_{-0.3}$ | $4.4^{+0.3}_{-0.3}$ | $4.1^{+0.3}_{-0.3}$ | $4.6^{+0.3}_{-0.3}$ |
| F_{640} | $1.49^{+0.16}_{-0.16}$ | $1.51^{+0.16}_{-0.16}$ | $1.52^{+0.16}_{-0.15}$ | $1.46^{+0.15}_{-0.15}$ |
| F_{706} | $0.21^{+0.15}_{-0.15}$ | $0.14^{+0.14}_{-0.14}$ | $0.17^{+0.15}_{-0.14}$ | $0.10^{+0.14}_{-0.10}$ |
| F_{667} | $1.23^{+0.16}_{-0.16}$ | $1.23^{+0.15}_{-0.16}$ | $1.25^{+0.15}_{-0.15}$ | $1.17^{+0.15}_{-0.15}$ |
| χ^2/dof | 84.2/101 | 92.6/102 | 88.0/102 | 94.7/103 |
| XMM-Newton/PN(2001): Correction factor = 2.6 | | | | |
| F_{pow} | $5.0^{+0.3}_{-0.3}$ | $5.1^{+0.3}_{-0.3}$ | $4.9^{+0.3}_{-0.3}$ | $5.0^{+0.3}_{-0.3}$ |
| F_{640} | $1.28^{+0.12}_{-0.11}$ | $1.32^{+0.11}_{-0.12}$ | $1.35^{+0.03}_{-0.06}$ | $1.34^{+0.11}_{-0.11}$ |
| F_{706} | $0.24^{+0.09}_{-0.10}$ | $0.21^{+0.10}_{-0.09}$ | $0.24^{+0.05}_{-0.03}$ | $0.23^{+0.10}_{-0.09}$ |
| F_{667} | $0.84^{+0.11}_{-0.11}$ | $0.87^{+0.11}_{-0.05}$ | $0.92^{+0.04}_{-0.03}$ | $0.90^{+0.09}_{-0.10}$ |
| χ^2/dof | 260.4/164 | 267.5/165 | 267.1/165 | 267.9/166 |

Note—Same as table 4.

ground levels.

3.3. The Constant 6.67 keV Line Flux

The most serious problem when comparing the line fluxes between different satellites or different instruments is the reliability of the cross-calibration of their relative efficiencies. The 6.67 keV line emission is due to the largely extended GCDX and a new SNR G 0.61 ± 0.01 , which contributes about 30% of the total 6.67 keV line emission in the Sgr B2 region. Therefore, the 6.67 keV line flux is time invariant and hence is a good cross-calibration line for the relative efficiencies of the Suzaku, XMM-Newton, Chandra, and ASCA observations. The constant flux hypothesis for the best-fit 6.67 keV line given in tables 2 and 3 is rejected with $\chi^2/\text{dof} = 56.3/8$, which indicates that there are significant systematic errors in the detection efficiencies of the ASCA, XMM-Newton, Chandra and Suzaku observations.

The nominal systematic errors for these satellites are: 13% for the ASCA SIS³, 5% for Chandra (Schwartz et al. 2000), 10% for EPIC (also the MOS flux is 10–15% higher than the PN (Carter & Read 2007)) and 10% for Suzaku (Serlemittos et al. 2007).

The 6.67 keV line flux history obtained by adding these systematic errors to the statistical errors are plotted in figure 3. The χ^2/dof value with a constant flux model is then 4.9/8, which is acceptable at a 70% confidence level. Therefore, as expected, the 6.67 keV line flux is constant, if systematic errors are taken into account.

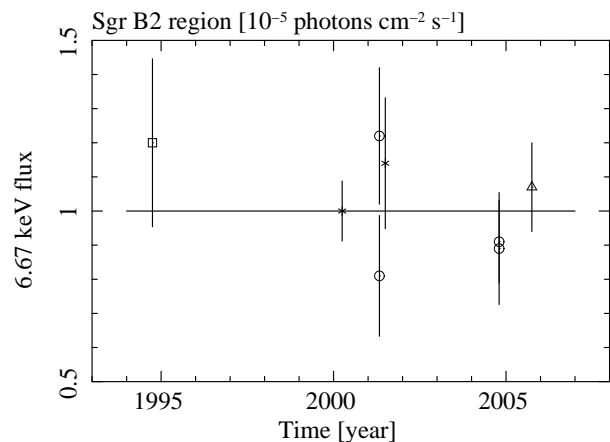


Fig. 3. The time trend of 6.67 keV line fluxes in the Sgr B2 region. In this plot, each error bar indicates one sigma including the statistical and systematic uncertainties. The Suzaku data are indicated by triangles, XMM-Newton MOS data by circles, Chandra data by asterisks, and ASCA data by squares. The average flux is shown by the solid horizontal line.

3.4. Time-Variable 6.40 keV Line

Unlike the 6.67 keV line, the 6.40 keV line emission is much more clumpy, hence it may not be time constant. To examine whether the 6.40 keV line from the Sgr B2 region is time variable or not, we performed a χ^2 test using the same procedure as those of the 6.67 keV line. For the case with no systematic errors, the constant flux hypothesis is rejected with $\chi^2/\text{dof} = 112.8/8$.

We next added the systematic errors in the same way as the 6.67 keV line case, and the constant flux hypothesis

³ See <http://heasarc.gsfc.nasa.gov/listserv/ascanews/msg00143.html>

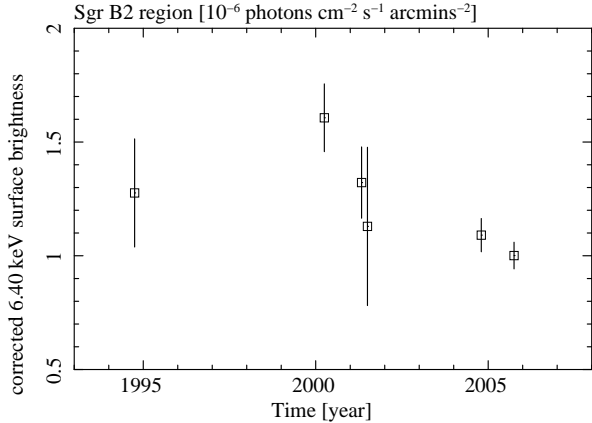


Fig. 4. The light curve of the corrected 6.40 keV line surface brightness in the Sgr B2 region. In this plot, each error bar indicates a 90% confidence limit.

was still rejected with $\chi^2/\text{dof} = 17.9/8$. Therefore, the 6.40 keV line flux is time variable.

Having confirmed that the 6.67 keV line is constant, we used it as a cross-calibrator. We introduced normalization factors for the detection efficiencies ($c \pm \delta c$) for the eight observations shown in table 6, where δc is a statistical error. These parameters are the ratios of the best-fit 6.67 keV line flux of each satellite to the averaged flux.

The best-fit 6.40 keV line fluxes were divided by these factors, and are referred to as the corrected 6.40 keV line flux. Since the MOS and PN fluxes should be consistent, we averaged these fluxes and errors. Figure 4 shows the corrected 6.40 keV line fluxes in each observation period. The 6.40 keV line flux varies significantly with $\chi^2/\text{dof} = 28.9/6$. The flux of the 2005 observation is about 60% that of 2000.

3.5. Sub-structures in the Sgr B2 region

In order to examine the morphology history of the 6.40 keV line, we made a surface brightness map of iron lines for each observation. Since the energy resolutions of Chandra or ASCA were not sufficiently good to separate the 6.40 keV line from the 6.67 keV line, all the images are in the 6–7 keV band. For the continuum flux subtraction from the 6–7 keV band flux, we assumed a power-law continuum of the photon index of 2.6, the best-fit Suzaku value, and estimated that the power-law continuum in the 6–7 keV band is 65% of the 5–6 keV band flux. After subtracting the continuum emission, we made the surface brightness maps using a pixel unit of 50-arcsec square, similar to the PSF of ASCA, which had the worst PSF among the four satellites.

Figures 5(a)–(d) show the surface brightness maps of the iron lines. The Suzaku and XMM-Newton images are relatively dim in the whole area compared to Chandra and ASCA, which is consistent with the spectral fitting result. In the Chandra image, a bright spot is found in the west, where a SNR candidate G 0.570–0.018 is located (Senda et al. 2002). We selected the brightest spot

named M 0.66–0.02 (solid circle in figure 5) from its position, which was termed the ‘‘Sgr B2 cloud’’ in previous papers, and G 0.570–0.018 (dashed circle in figure 5). We then examined the 6.40 keV flux changes from these two spots. Since the Chandra data in 2001 did not have enough statistics for the analysis, we excluded this data hereafter.

3.5.1. M 0.66–0.02

We extracted the spectra of M 0.66–0.02 (Sgr B2 cloud) from the solid circle with a radius of 3.2 arcmin in figure 5 and subtracted the blank-sky data in the same detector position. In the ASCA image, the peak position of M 0.66–0.02 is different from those in the others. It is not clear whether this shift is due to a relatively large error of the ASCA astrometry (no fine-tuning of the ASCA astrometry was performed, see Section 2.4) or due to a real shift in the variable 6.40 keV line. Therefore, in the ASCA analysis, we selected two circles for M 0.66–0.02, at the same as the position in the original coordinate of Suzaku, XMM-Newton, and Chandra (P) and at the center on the peak of the SIS image (Q).

As described in Section 3.2, the dependences of the line fluxes on the continuum models and on the uncertainties of NXB (systematic errors) are not larger than the statistical errors of the Sgr B2 region. Since the statistical error of the line flux from M 0.66–0.02 is larger than that of the Sgr B2 region, these systematic errors can be neglected. We nevertheless attempted the same analysis as the Sgr B2 region and found no difference within different continuum modeling and/or background subtractions. We therefore estimated the line fluxes using the continuum models of N_{H} and Γ free. The ASCA/SIS fluxes of the 6.40 keV line were $0.99^{+0.13}_{-0.14}$ for the spectrum region ‘P’, and $0.93^{+0.11}_{-0.15} \times 10^{-4}$ photons $\text{cm}^{-2} \text{s}^{-1}$ for that of region ‘Q’. These fluxes are consistent within the statistical error, hence we used the result of region ‘P’. The best-fit spectra and parameters are shown in figure 6 and table 7, respectively.

However, cross-calibration errors for the efficiencies between the four satellites may not be neglected. We therefore corrected the 6.40 keV fluxes using the correction factors shown in table 6, which are derived from the 6.67 keV line flux in the Sgr B2 region (Section 3.5). The results are plotted in figure 7. This time history is similar to that of the Sgr B2 region (the whole region) (figure 4). The constant flux hypothesis is rejected with $\chi^2/\text{dof}=30.7/6$. The flux in 2000 is 1.5 times higher than those in 2004 and 2005, and declines in 2001.

3.5.2. G 0.570–0.018

G 0.570–0.018 is a diffuse source extending to about 10 arcmin (Senda et al. 2002). We extracted the 6.40 keV flux from G 0.570–0.018 (the dashed circle with a radius of 2.5 arcmin in figure 5) in the same way as M 0.66–0.02. Since the spectra do not have enough statistics to derive Fe I $K\beta$ (7.06 keV) line, the intensity of $K\beta$ was fixed to 12.5% that of $K\alpha$ (Kaastra & Mewe 1993). Using the same method as Section 3.5.1 except for the fixed line ratio, we fitted the Suzaku spectra with N_{H} and Γ free

Table 6. The normalization factors of the detection efficiency for the eight observations

| Suzaku XIS(2005) | XMM-Newton MOS(2004) PN(2004) | | XMM-Newton MOS(2001) PN(2001) | | Chandra ACIS(2001) | Chandra ACIS(2000) | ASCA SIS(1994) |
|---------------------|----------------------------------|-----------------|----------------------------------|-----------------|-----------------------|-----------------------|-------------------|
| 1.05 ± 0.05 | 0.91 ± 0.08 | 0.89 ± 0.06 | 1.25 ± 0.14 | 0.83 ± 0.11 | 1.12 ± 0.29 | 0.99 ± 0.07 | 1.19 ± 0.18 |

Note—Parentheses indicate in the 90% confidence limit.

Normalization factors and their errors of the detection efficiency derived from the ratio of the best-fit 6.67 keV line flux in the Sgr B2 region obtained with each observation to the averaged flux.

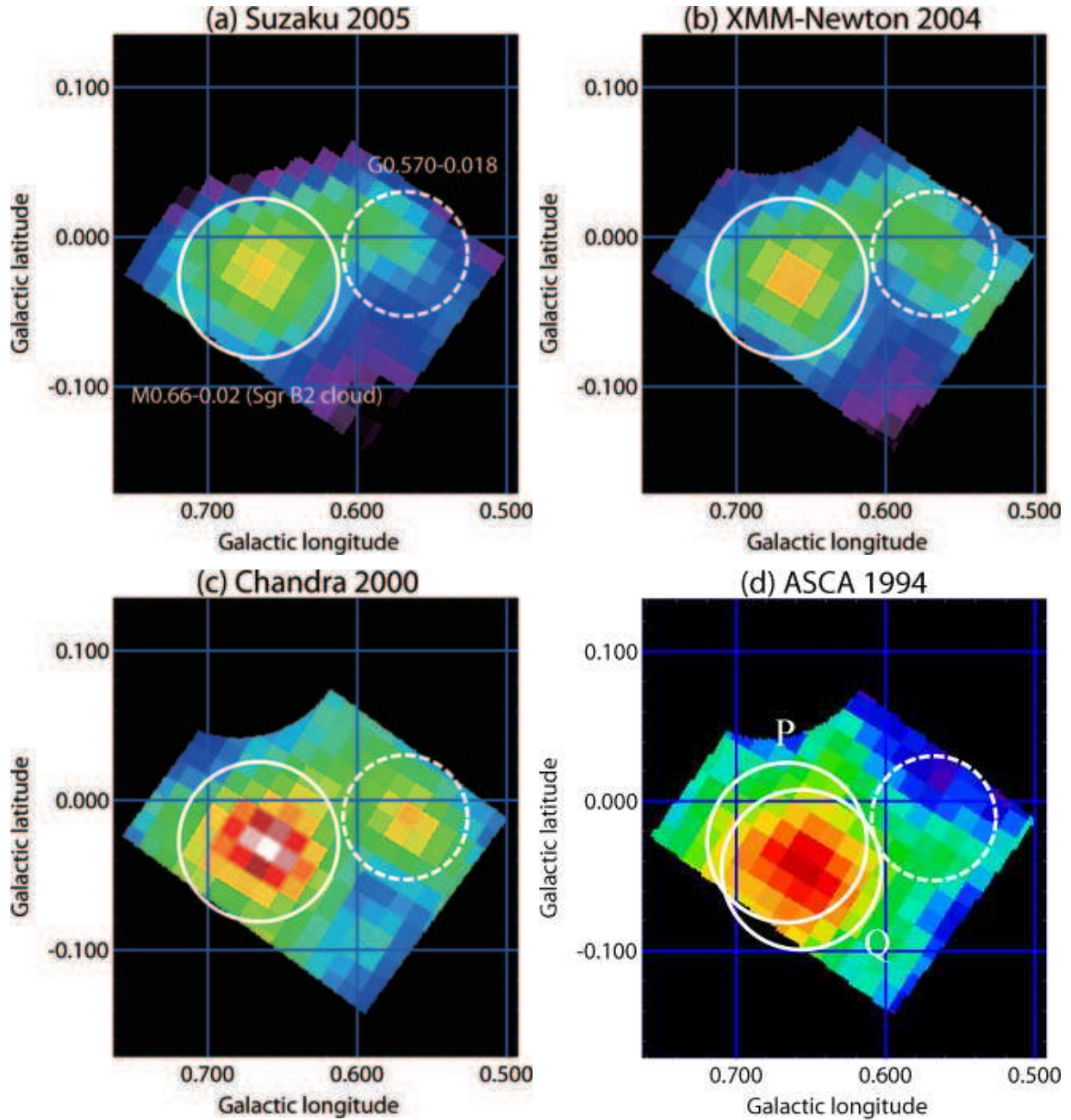


Fig. 5. Surface brightness maps of iron lines obtained with (a) Suzaku XIS 2005, (b) XMM-Newton MOS and PN 2004, (c) Chandra ACIS-I 2000, and (d) ASCA SIS 1994. Pixel size is $50'' \times 50''$ in each case

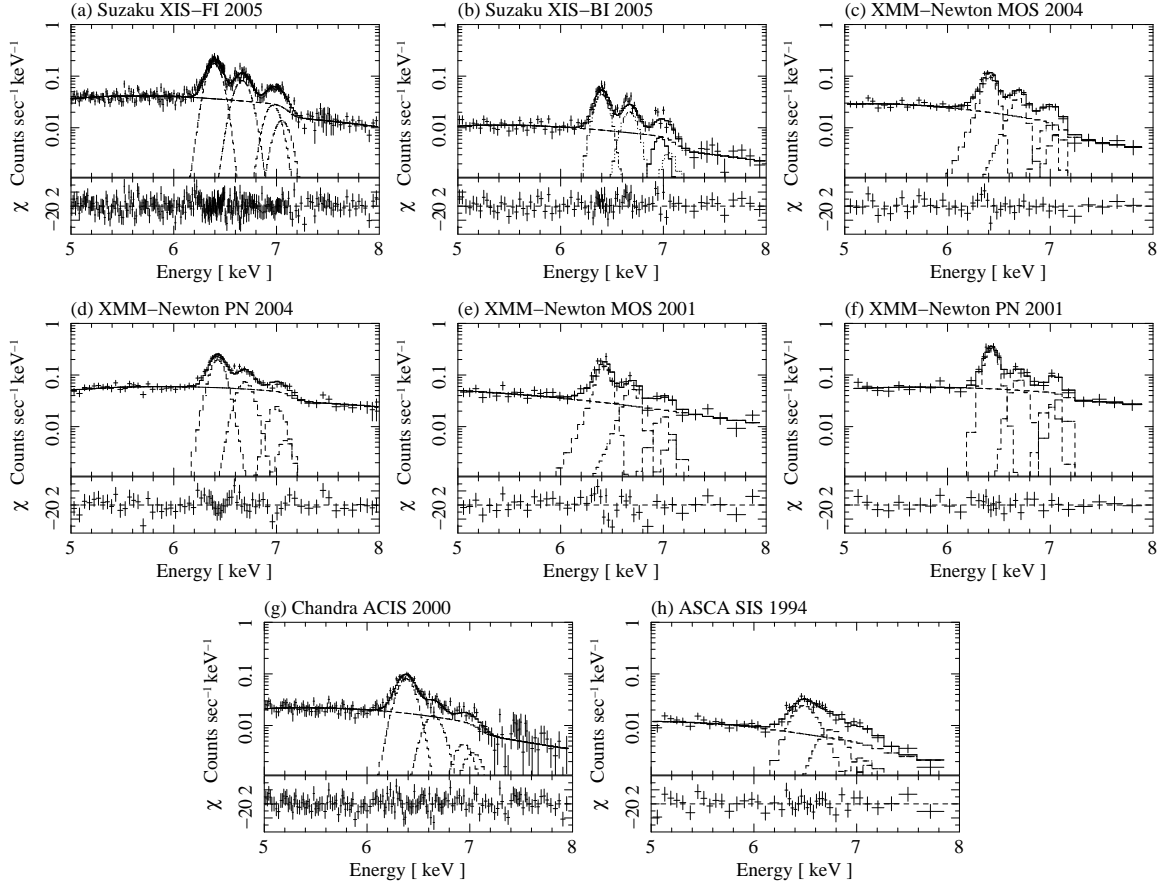


Fig. 6. Spectra for M 0.66–0.02 obtained with Suzaku XIS FI sensors (a) and BI sensor (b) in 2005, XMM-Newton MOS (c) and PN (d) in 2004, (e) and (f) in 2001, Chandra ACIS-I (g) in 2000, and ASCA SIS (h) in 1994. The solid lines indicate the best-fit models.

Table 7. The best-fit parameters of M 0.66–0.02

| Observatory Detector | Suzaku XIS(2005) | XMM-Newton MOS(2004) | XMM-Newton PN(2004) | XMM-Newton MOS(2001) | XMM-Newton PN(2001) | Chandra ACIS(2000) | ASCA SIS(1994) |
|-----------------------------|------------------------|-------------------------|------------------------|-------------------------|------------------------|------------------------|------------------------|
| —Continuum— | | | | | | | |
| N_{H} | $5.0^{+0.5}_{-0.3}$ | $5.4^{+2.1}_{-2.0}$ | $3.7^{+1.1}_{-1.1}$ | $0.2^{+2.4}_{-0.2}$ | $2.5^{+2.8}_{-2.5}$ | $4.3^{+1.1}_{-1.6}$ | $3.0^{+2.9}_{-1.4}$ |
| Γ | $3.0^{+0.3}_{-0.3}$ | $3.2^{+0.5}_{-1.0}$ | $1.7^{+0.2}_{-0.3}$ | $0.1^{+1.0}_{-0.5}$ | $1.2^{+1.1}_{-1.1}$ | $1.2^{+0.5}_{-0.9}$ | $1.7^{+1.9}_{-1.4}$ |
| F_{pow} | $2.0^{+0.1}_{-0.1}$ | $1.6^{+0.1}_{-0.1}$ | $2.4^{+0.1}_{-0.1}$ | $3.0^{+0.2}_{-0.2}$ | $2.4^{+0.2}_{-0.2}$ | $2.7^{+0.1}_{-0.1}$ | $2.3^{+0.2}_{-0.2}$ |
| —Neutral iron lines— | | | | | | | |
| F_{640} | $0.66^{+0.02}_{-0.02}$ | $0.58^{+0.04}_{-0.04}$ | $0.57^{+0.04}_{-0.04}$ | $0.92^{+0.11}_{-0.11}$ | $0.82^{+0.10}_{-0.09}$ | $1.00^{+0.05}_{-0.06}$ | $0.99^{+0.13}_{-0.14}$ |
| F_{706} | $0.06^{+0.04}_{-0.04}$ | $0.08^{+0.04}_{-0.04}$ | $0.02^{+0.03}_{-0.02}$ | $0.05^{+0.09}_{-0.05}$ | $0.11^{+0.08}_{-0.07}$ | $0.06^{+0.06}_{-0.04}$ | $0.12^{+0.13}_{-0.11}$ |
| —highly ionized iron lines— | | | | | | | |
| F_{667} | $0.36^{+0.02}_{-0.02}$ | $0.29^{+0.04}_{-0.04}$ | $0.25^{+0.03}_{-0.03}$ | $0.42^{+0.09}_{-0.09}$ | $0.26^{+0.08}_{-0.07}$ | $0.25^{+0.04}_{-0.04}$ | $0.42^{+0.13}_{-0.13}$ |
| F_{697} | $0.12^{+0.03}_{-0.02}$ | 0.10^a | 0.08^a | 0.14^a | 0.09^a | 0.08^a | 0.14^a |
| δ_{Gain} | 0(fix) | 0(fix) | 23^{+6}_{-4} | 0(fix) | 23^{+13}_{-17} | -19^{+8}_{-3} | 81^{+21}_{-11} |
| χ^2/dof | 348.4/354 | 36.9/40 | 71.3/68 | 35.3/38 | 16.6/27 | 142.1/144 | 36.1/37 |

Note—Same as table 3.

^a The intensity of Fe XXVI K α is fixed at 34% of that of Fe XXV K α obtained with Suzaku.

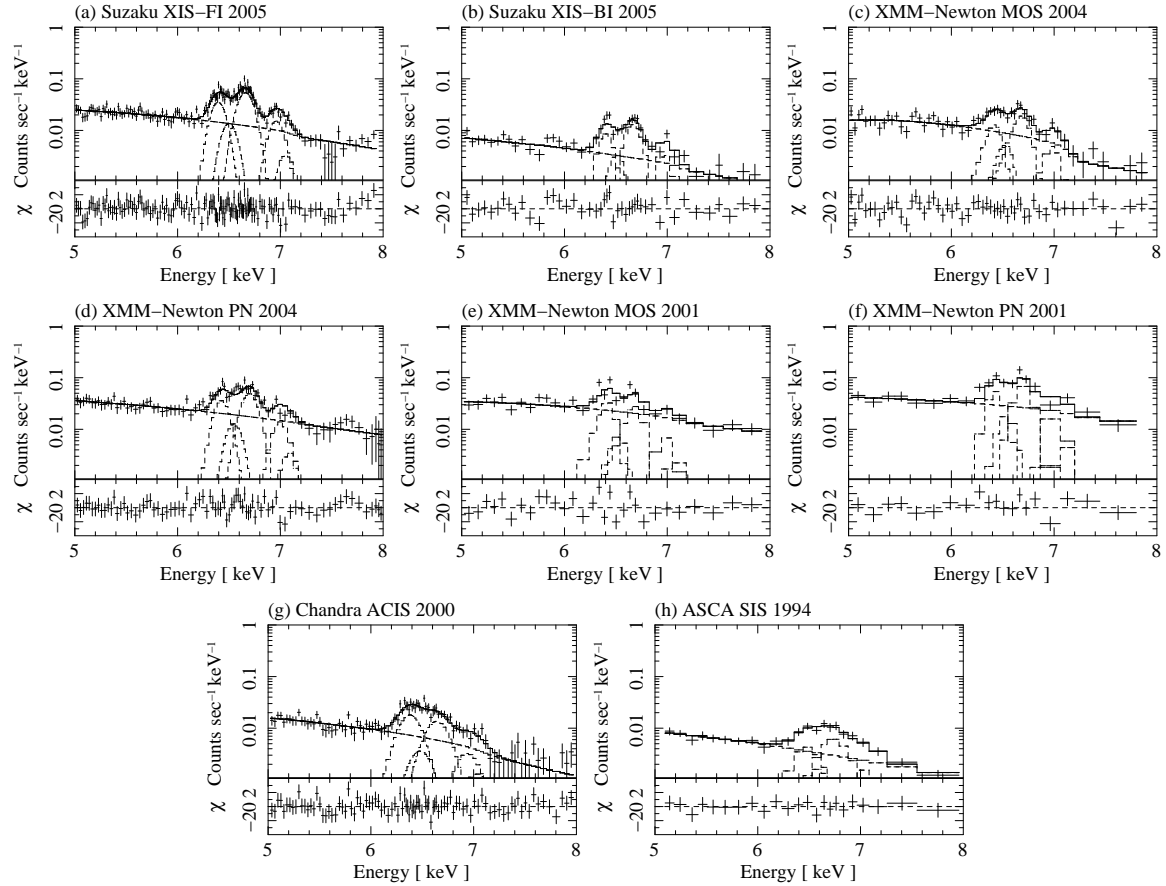


Fig. 8. Spectra for G 0.570–0.018 obtained with Suzaku XIS FI sensors (a) and BI sensor (b) in 2005, XMM-Newton MOS (c) and PN (d) in 2004, (e) and (f) in 2001, Chandra ACIS-I (g) in 2000, and ASCA SIS (h) in 1994. The solid lines indicate the best-fit models.

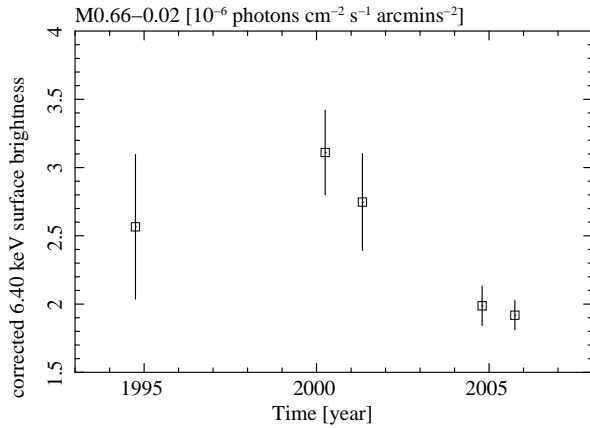


Fig. 7. The light curve of the 6.40 keV line surface brightness from M0.66–0.02 (Sgr B2 cloud). In this plot, each error bar indicates a 90% confidence limit.

model. We obtained 6415 eV as the line centroid of the 6.40 keV line, which is 15 eV higher than the values obtained in the other region. We then refitted the spectra with the line centroids fixed at the values for the Sgr B2 region (table 2) and found significant residuals in the 6.4–6.6 keV band. We added one Gaussian function in this energy band, and obtained an acceptable fit. The centroid of the additional line is 6505 eV, which is consistent with the value reported by Senda et al. (2002). From the energy centroid, this line is likely to be due to FeXX-K α . Assuming a thin-thermal plasma, the temperature of the most prominent emission of this line is 1.1 keV, a typical temperature of an SNR, which led Senda et al. (2002) to propose a new SNR in highly non-equilibrium ionization.

Since the flux of the 6.51 keV line is due to highly ionized iron and the flux is likely to be time constant, the flux ratio among the highly ionized iron lines is fixed in the following analysis. The best-fit spectra and parameters are shown in figure 8 and table 8, respectively.

We corrected the 6.40 keV fluxes using the correction factors as we did for M0.66–0.02. Figure 9 shows the time trend of the 6.40 keV line from G 0.570–0.018, which indicates a clear variability in the 6.40 keV line emission. A constant flux hypothesis is marginally rejected with $\chi^2/\text{dof} = 13.2/6$.

Table 8. The best-fit parameters of G 0.570–0.018

| Observatory | Suzaku | XMM-Newton | XMM-Newton | XMM-Newton | Chandra | ASCA | |
|------------------------|------------------------|------------------------|------------------------|------------------------|------------------------|------------------------|------------------------|
| Detector | XIS(2005) | MOS(2004) | PN(2004) | MOS(2001) | PN(2001) | ACIS(2000) | SIS(1994) |
| —Continuum— | | | | | | | |
| N_{H} | $1.5^{+1.3}_{-1.0}$ | $6.2^{+1.6}_{-2.5}$ | $0.4^{+1.7}_{-0.4}$ | $1.3^{+1.4}_{-1.3}$ | $1.5^{+3.6}_{-1.5}$ | $2.0^{+2.7}_{-2.0}$ | $0.2^{+3.4}_{-0.2}$ |
| Γ | $2.6^{+0.6}_{-0.5}$ | $4.1^{+1.9}_{-1.6}$ | $1.8^{+0.8}_{-0.6}$ | $0.5^{+1.2}_{-0.9}$ | $2.0^{+1.6}_{-1.2}$ | $2.0^{+1.4}_{-0.6}$ | $1.2^{+1.5}_{-0.8}$ |
| F_{pow} | $1.1^{+0.1}_{-0.1}$ | $1.1^{+0.1}_{-0.1}$ | $1.3^{+0.1}_{-0.1}$ | $1.9^{+0.1}_{-0.1}$ | $1.2^{+0.1}_{-0.1}$ | $1.2^{+0.1}_{-0.1}$ | $0.9^{+0.1}_{-0.1}$ |
| —Neutral iron lines— | | | | | | | |
| F_{640} | $0.16^{+0.03}_{-0.05}$ | $0.11^{+0.04}_{-0.04}$ | $0.14^{+0.03}_{-0.03}$ | $0.18^{+0.06}_{-0.06}$ | $0.19^{+0.06}_{-0.06}$ | $0.26^{+0.04}_{-0.04}$ | $0.12^{+0.05}_{-0.05}$ |
| —Ionized iron lines— | | | | | | | |
| F_{667} | $0.29^{+0.02}_{-0.02}$ | $0.20^{+0.04}_{-0.04}$ | $0.22^{+0.03}_{-0.03}$ | $0.18^{+0.06}_{-0.06}$ | $0.23^{+0.06}_{-0.06}$ | $0.25^{+0.03}_{-0.03}$ | $0.20^{+0.04}_{-0.02}$ |
| F_{651} | $0.07^{+0.03}_{-0.02}$ | 0.05^d | 0.06^d | 0.04^d | 0.05^d | 0.06^d | 0.05^d |
| δ_{Gain} | 0(fix) | 0(fix) | 35(fix) | 0(fix) | 33(fix) | –18(fix) | 71(fix) |
| χ^2/dof | 192.3/181 | 56.1/51 | 70.8/78 | 40.9/25 | 21.0/15 | 82.4/93 | 6.8/18 |

Note—Same as table 3.

^d Fixed at the value and flux ratio against Fe XXV $K\alpha$ line obtained with Suzaku.

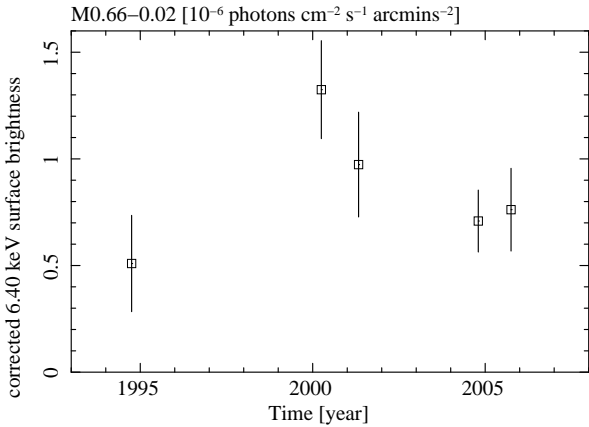


Fig. 9. The light curve of the 6.40 keV line surface brightness from G 0.570–0.018. In this plot, each error bar indicates a 90% confidence limit.

Senda et al. (2002) mentioned that G 0.570–0.018 is a simple SNR candidate, but the 6.40 keV variability suggests that G 0.570–0.018 includes an XRN (see Discussion). In fact, Miyazaki & Tsuboi (2000) reported a flux peak of the CS ($J=1-0$) line emission at $(l, b) = (0^\circ 601, -0^\circ 025)$, which indicates the presence of a molecular cloud. The light curve of G 0.570–0.018 is similar to that of M 0.66–0.02. Hence the distances of the two clouds from Sgr A* are the same. G 0.570–0.018 may be located in front of M 0.66–0.02 with some off-sets of the line of sight.

4. Discussion

The 6.40 keV line is K-shell emission of neutral or low-ionization iron. Hence, since cool gases such as molecular clouds cannot emit X-ray photons, the 6.40 keV line is due to illumination by external sources of either X-rays or charged particles. The analyses of ASCA, Chandra and Suzaku (Koyama et al. 1996, Murakami et al. 2001b,

Koyama et al. 2007b) revealed strong Fe I $K\alpha, \beta$ lines and deep Fe K edge, which supports an X-ray origin. However, an electron origin cannot be excluded if the iron abundance is higher than the solar value by a factor of 3–4 (Yusef-Zadeh et al. 2007) and the X-ray spot is at the back-side of the molecular clouds.

The time variability of the 6.40 keV line in the Sgr B2 region has already been reported by Koyama et al. (2008a) from the Chandra (2000) to the Suzaku (2005) observations. A similar time variability has also been reported for the other cloud near Sgr A* by Muno et al. (2007) and Koyama et al. (2008b), which are the time variabilities of a few years span. In this paper, we have confirmed the time variability with a longer time scale (~ 10 years) from the Sgr B2 region.

This time variability is also found in the sub-structures, M 0.66–0.02 and G 0.570–0.018. The sizes of these two sources are a few tens of light years, which is comparable to the variation time scale. These time variabilities are the clearest evidence for X-ray origin, because it is difficult to change the flux of any charged particle in a large region (a few 10 light-years) within a few 10 years.

If the origin is X-ray irradiation, the observed 6.40 keV flux requires a bright source with a luminosity of more than 10^{37} erg s^{-1} assuming the source is located near the Sgr B2 region in the distance of 8.5 kpc. Point sources in the GC region have been catalogued by many satellites, but no source has been brighter than 10^{37} erg s^{-1} in a time scale of ten years. Thus, we conclude that the most probable source is the massive black hole Sgr A*.

In this scenario, the light curves of the 6.40 keV line flux in the molecular clouds can be used as a tracer of the light curve of Sgr A* in the past, like a time-delayed echo. Since the light travel time between Sgr A* and the Sgr B2 region is ~ 300 years, we already proposed that Sgr A* was X-ray bright ($\sim 10^{39}$ erg s^{-1}) 300 years ago. Our new results indicate that the X-rays have been variable over a time scale of a few tens of years. The light curve of the 6.40 keV line is not the real history of Sgr A*. It is smeared out if the size of the reflection (fluorescence)

cloud is comparable or larger than the light-cross scale. Then, (1) even if the real light curve is pulse-like (delta-function), the observed light curve of the fluorescent line is smoothed on a scale of the light crossing time of the cloud, or (2) if the cloud is very small (like a point source), the observed light curve is the real history of the incident X-rays. The high-resolution Chandra image (Koyama et al. 2008a) revealed that the fluorescent line emission has a complex structure with bright peak of a scale of less than 1 arcmin (~ 6 light years). Therefore, a realistic situation lies between cases (1) and (2), so that the observed light curve is moderately smeared-out. This means that the observed variability amplitude is a lower limit of the actual one, although they do not differ largely from each other. Hereafter, we discuss the evolution of the Sgr A* outburst based on the observed light curve. The averaged decay rate of the 6.40 keV line is 60% in 10 years, hence the half-decay time is ~ 15 years. If this decay time has been constantly folded for 300 years, the X-ray luminosity after 300 years becomes 10^{33-34} erg s $^{-1}$, which is consistent with the observed value in the present. We hence propose that 300 years ago, Sgr A* experienced a giant flare and then entered a decay phase that continued to the present.

5. Summary

We summarize the results as follows:

1. We have extensively studied the spectra of the Sgr B2 region, assuming various continuum models, backgrounds and uncertainties of the relative efficiencies of Suzaku, XMM-Newton Chandra, and ASCA. We then found that the 6.40 keV line fluxes are time variable.
2. We found the time variability of the individual clouds, M 0.66–0.02 and G 0.570–0.018.
3. The time histories of the 6.40 keV line flux are similar for all the sources, and exhibit their brightest peak in 2000, decline in 2001 and finally fall to 60% in 2005.
4. The 6.40 keV variability of the diffuse source G 0.570–0.018 suggests that this source is a candidate for an XRN.
5. The variability of the 6.40 keV line indicates that the GC black hole Sgr A* experienced a large flare 300 years ago and entered a decay phase.

The authors thank all of the Suzaku team members, especially H. Uchiyama, H. Nakajima, H. Yamaguchi, and H. Mori for their support and for providing useful information on the XIS performance. This work is supported by Grant-in-Aids from the Ministry of Education, Culture, Sports, Science and Technology (MEXT) of Japan, the 21st Century COE "Center for Diversity and Universality in Physics", Scientific Research A (KK), Priority Research Areas in Japan "New Development in Black Hole Astronomy" (TGT), and Grant-in-Aid for Young Scientists B (HM) HM is also supported by the Sumitomo Foundation, Grant for Basic Science Research

Projects, 071251, 2007. TI is supported by a JSPS Research Fellowship for Young Scientists.

References

- Baganoff, F. K., et al. 2001, *Nature*, 413, 45
 Carter, J. A., & Read, A. M. 2007, *A&A*, 464, 1155
 Eisenhauer, F., et al. 2005, *ApJ*, 628, 246
 Ghez, A. M., Salim, S., Hornstein, S. D., Tanner, A., Lu, J. R., Morris, M., Becklin, E. E., & Duchêne, G. 2005, *ApJ*, 620, 744
 Kaastra, J. S., & Mewe, R. 1993, *A&AS*, 97, 443
 Koyama, K., Maeda, Y., Sonobe, T., Takeshima, T., Tanaka, Y., & Yamauchi, S. 1996, *PASJ*, 48, 249
 Koyama, K. et al. 2007a, *PASJ*, 59, S23
 Koyama, K. et al. 2007b, *PASJ*, 59, S221
 Koyama, K. et al. 2007c, *PASJ*, 59, S245
 Koyama, K. et al. 2008a, *PASJ*, 60, (in press) (astro-ph/0711.2853)
 Koyama, K. et al. 2008b, *PASJ*, submitted (#3307)
 Mitsuda, K. et al. 2007, *PASJ*, 59, S1
 Miyazaki, A., & Tsuboi, M. 2000, *ApJ*, 536, 357
 Munro, M. P., et al. 2003, *ApJ*, 589, 225
 Munro, M. P., Baganoff, F. K., Brandt, W. N., Park, S., & Morris, M. R. 2007, *ApJL*, 656, L69
 Murakami, H., Koyama, K., Tsujimoto, M., Maeda, Y., & Sakano, M. 2001, *ApJ*, 550, 297
 Murakami, H., Koyama, K., & Maeda, Y. 2001, *ApJ*, 558, 687
 Nobukawa, M., et al. 2008, *PASJ*, 60, (in press) (astro-ph/0712.0877)
 Predehl, P., Costantini, E., Hasinger, G., & Tanaka, Y. 2003, *Astronomische Nachrichten*, 324, 73
 Reid, M. J., Schneps, M. H., Moran, J. M., Gwinn, C. R., Genzel, R., Downes, D., & Roennaeng, B. 1988, *ApJ*, 330, 809
 Schwartz, D. A., et al. 2000, *Proc. SPIE*, 4012, 28
 Senda, A., Murakami, H., & Koyama, K. 2002, *ApJ*, 565, 1017
 Serlemitsos, P. et al. 2007, *PASJ*, 59, S9
 Strüder, L., et al. 2001, *A&A*, 365, L18
 Turner, M. J. L., et al. 2001, *A&A*, 365, L27
 Tatischeff, V. 2003, in *Final Stage of Stellar Evolution*, ed. C. Motch & Hameury (EAS publication Series vol.7), 79 (astro-ph/0208397v1)
 Weisskopf, M. C., Brinkman, B., Canizares, C., Garmire, G., Murray, S., & Van Speybroeck, L. P. 2002, *PASP*, 114, 1
 Weisskopf, M. C., et al. 2003, *Experimental Astronomy*, 16, 1
 Yusef-Zadeh, F., Munro, M., Wardle, M., & Lis, D. C. 2007, *ApJ*, 656, 847